Optimisation of anatase TiO_2 thin film growth on $LaAlO_3$(001) using pulsed laser deposition

K. Krupski[1,*], A.M. Sanchez[1], A. Krupski[1,2], C.F. McConville[1]

[1] Department of Physics, University of Warwick, Coventry CV4 7AL, UK

[2] Faculty of Science, SEES, University of Portsmouth, Portsmouth PO1 3QL, UK

* Corresponding author: (K. J. Krupski), E-Mail: k.j.krupski@warwick.ac.uk

ABSTRACT

Optimisation of epitaxial anatase TiO_2 thin films grown on $LaAlO_3$(001) substrates was performed using ultra-high vacuum based pulsed laser deposition (PLD) and studied by in-situ reflection high-energy electron diffraction (RHEED). In addition, ex-situ X-ray diffraction (XRD), atomic force microscopy (AFM), and scanning transmission electron microscopy (STEM) were performed to characterise the bulk properties of these thin films. The deposited TiO_2 thin film is demonstrated to have anatase phase and bonded directly to the $LaAlO_3$(001) substrate. In a separate ultra-high vacuum system low-energy electron diffraction (LEED) and scanning tunnelling microscopy (STM) measurements were performed and a well-ordered two-domain (1×4) and (4×1) reconstruction of anatase surface was observed. Analysis of the STM measurements indicates the coexistence of atomic steps of both 2.5 Å and 5.0 Å, confirming the existence of two TiO_2 domains. The atomic resolution STEM images reveal that the $TiO_2/LaAlO_3$ interface to be terminated with LaO layer and that the anatase-TiO_2 reconstruction was found to be stable during the film growth.

Keywords: Anatase; Titanium dioxide; Lanthanum aluminate; Pulsed laser deposition (PLD); Reflection high-energy electron diffraction (RHEED); Low-energy electron diffraction (LEED); X-ray diffraction (XRD); Atomic force microscopy (AFM); Scanning tunnelling microscopy (STM); Scanning transmission electron microscopy (STEM); Growth; Thin film growth.

1. INTODUCTION

Titania, TiO_2, has a wide range of applications and a large number of extremely interesting properties. A key 'low-tech' application that stems not only from its optical properties, but also its non-toxicity, is use as a whitening agent in paints and paper. However, applications that more directly stem from its surface properties, as well as the bulk, arise in heterogeneous catalysis including photo-catalysis [1-2], the photovoltaic effect [3-4], and collar cells [5], and it is these applications that are at least part of the reason why TiO_2 is almost certainly the most studied of all oxides surface [6]. Until now, the majority of studies of TiO_2 have been performed on the rutile phase [7-9]. Rutile is the thermodynamically equilibrium phase of TiO_2 at ambient pressures, but two other isomorphs, anatase and brookite also occur naturally. Crucially anatase appears to be the equilibrium phase for small particles with dimension less than 11 nm [2]. It is therefore generally believed that anatase is the active component in many titania based heterogeneous catalysts [4, 10] and in current solar cell applications based on nano-crystalline material. As such, there is a clear need to gain a better understanding of the anatase surface structure and the role of the TiO_2 growth conditions (e.g. substrate temperature, oxygen pressure - during growth and annealing, etc.). Thin films of TiO_2 can be formed on a wide variety of substrates including oxide surfaces such as: MgO [11], $SrTiO_3$ [11-12], and $LaAlO_3$ [11-13]. Different deposition methods such as reactive sputter deposition [14], oxygen plasma assisted molecular beam epitaxy (PAMBE) [12,15] or pulsed laser deposition (PLD) [13,16-22] have all been used to fabricate the anatase phase. Until now of the substrates examined, $LaAlO_3$ (LAO) gives the best coherency owing to its relatively small lattice mismatch with anatase. In the bulk phase, anatase TiO_2 has a tetragonal structure with a lattice parameters a = 0.3776 nm and c = 0.9486 nm, while $LaAlO_3$ can be described as a pseudo-cubic perovskite with a lattice parameter a = 0.3792 nm, leading to a mismatch of only 0.4% when TiO_2 is grown epitaxially on the (001) surface

of $LaAlO_3$ [23**]**. While most studies have focused on the bulk structure of the anatase films, studies have also investigated optimization of film growth to obtain good surface properties of anatase TiO_2(001), i.e. atomically smooth terraces with well-defined monoatomic step-structures. In oxygen plasma-assisted MBE, well defined surface structures were obtained for low growth rates (0.003–0.011 nm/s) at growth temperatures between 550 and 650 °C [24]. Under these conditions, a characteristic (4×1) reconstruction of the anatase TiO_2(001) surface [25-27] was observed in both reflection high-energy electron diffraction and low-energy electron diffraction measurements [28-29]. In one such study using low-energy ion emission [28], it was proposed that this reconstruction is based on (103) nano-facets of TiO_2, but later theoretical calculations of the surface energy for a range of surface orientations concluded that the (103) face is a high energy surface, and therefore rather unlikely [30].

The aim of the present study is the optimisation of the PLD growth parameters to generate smooth, flat surfaces and a well-defined interface between film and substrate. Bulk and surface characterization of the anatase-TiO_2(001)-(4×1) films on $LaAlO_3$(001) using RHEED, LEED, X-ray diffraction, atomic force microscopy (AFM), scanning tunnelling microscopy (STM), and scanning transmission electron microscopy (STEM).

2. EXPERIMENTAL

The thin films were prepared by pulsed laser deposition in an ultra-high vacuum (UHV) system with a base pressure 2×10^{-9} mbar, equipped with high-pressure RHEED and using a 248 nm KrF laser (Coherent, USA). TiO_2 ablation targets were made of anatase TiO_2 powder with 99.99% purity and mounted on a rotating carousel. During deposition, high purity oxygen was supplied to a pressure of 5.4×10^{-9} mbar, while the sample to target distance was around 4.7 cm. For the growth of anatase-TiO_2(001) thin films, $LaAlO_3$(001) substrates were used (Pi-KEM Ltd). The standard substrate preparation method involved ultrasonic cleaning,

first in acetone and next in ethanol for 10 min each. Substrates were mounted side-by-side on tantalum plates and placed into the UHV deposition chamber through a load-lock. All substrates were pre-annealed immediately before growth at the deposition temperature in an oxygen atmosphere of 5.4×10^{-9} mbar for one hour. The structure of the as-grown films was evaluated in-situ by RHEED during and immediately following deposition, and ex-situ with X-ray diffraction (45eV, 40mA, X'Pret PANalytical). All XRD scans were performed between 20° and 120° with the step of 0.02°. The surface topography of the deposited films was studied in-air using AFM in non-contact mode. The LEED and STM measurements were carried out at room temperature in the second stainless steel ultra-high vacuum chamber with a base pressure of 5.0×10^{-11} mbar. $TiO_2/LaAlO_3(001)$ samples were transferred between PLD/RHEED and LEED/STM chambers without breaking UHV conditions with the use UHV suitcase. All STM measurements were performed with the use of electrochemically etched W (99.99%) tips (diameter 0.5 mm, length 3.5 mm) [31]. All STM images were recorded in constant current mode and processed by the WSXM image-processing software [32]. The electron transparent specimen was prepared using conventional cross-section sample preparation methodology. The material was back-thinned to approximately 100 μm before cleaved and mounted on a support grid. Afterwards it was mechanically thinned to approximately 20 μm and ion-milled to electron transparency using Ar^+ ions at 6 kV and a beam incidence angle of 3° (cooled). A final low-energy 'clean' of the sample at 2 kV was employed to minimize amorphous surface layers. The Annular Dark Field images were recorded using a double CEOS aberration-corrected Jeol ARM-200F operation at 200kV. A convergence semi-angle of 22 mrad was used with a JEOL ADF detector with inner and outer collection semi-angle of 45 and 180 mrad, respectively.

3. RESULTS AND DISCUSSION

In order to evaluate the quality of the anatase thin film grown by PLD, a variety of different parameters were varied including: sample temperature; KrF laser energy and fluence; pulse frequency; and the sample-target distance (see Table 1). It was found that epitaxial anatase-TiO_2 thin film growth was observed for substrate temperatures between 620 and 700°C, and for oxygen partial pressures of $10^{-5} \leq p_{O2} \leq 10^{-2}$ mbar. Figure 1. demonstrates the quality of the anatase-TiO_2 thin films using in-situ RHEED, AFM, and XRD. The X-ray diffraction and high resolution X-ray diffraction (HRXRD) data were taken along the surface normal and rocking curve data experiments, respectively. The thicknesses of the TiO_2 films ranged from 7.64 nm to 100.26 nm as estimated by using rocking curves, X-ray reflectivity (XRR) and STEM methods, respectively (Table 1). The RHEED pattern in Figure 1(a) for the KrF laser energy = 43 mJ shows three weak additional streaks between the primary (intensity) spots on the 0^{th} Laue circle. The diffraction spots become streakier, possible indicating a roughening of the surface and some kind of heterogeneous growth mode which often occurs in oxide films. That is consistent with the AFM data, Figure 1(a), where 3D TiO_2 clusters are observed (marked by arrows) as a result of the possible initial miss-matched growth of TiO_2 on the $LaAlO_3$(001) substrate. The TiO_2 surface roughness in this case is equal to 1.65 nm. XRD scan shows two well defined peaks at 39.23° for (004) and 82.45° for (008) corresponding to the anatase phase. No fringe maxima were observed in HRXRD. In Figure 1(b) results for changed distance between sample and target are presented, Table 1. The RHEED pattern shows brighter than for previous sample three additional streaks and diffraction spots corresponding to 3D clusters (observed in AFM). These diffraction spots can be visible because the sample thickness is around 9.5 nm (Table 1), and it is possible that the bulk lattice parameters of substrate and film influence to the specular RHEED intensity. Fig. 1(c) presents results of sample which was annealed before growing for different oxygen pressure

= 0.1 mbar. RHEED reflection shows very weak streaks suggesting that the surface is mostly covered by an amorphous TiO_2 phase. Polycrystalline rings starts to become visible in RHEED. However, distinct spots are still visible on some of the rings, which suggest that the growth of TiO_2 is not completely random. In that case, the largest 3D TiO_2 clusters were observed by AFM. The sample shown in Fig. 1(d) was prepared with a substrate temperature of T = 670°C and further 3D islands were observed. However, the streaks in the RHEED are the weakest, which means that more of the surface is covered by the amorphous TiO_2 phase. Figure 1(e) shows a completely amorphous film with the 3D clusters grown on top. The measured film thickness and surface roughness were equal to 100.3 nm and 9.3 nm, respectively. In Figure 1(f) results of TiO_2 growth with a laser pulse frequency 8 Hz are shown. The XRD 2θ-θ scan shows no anatase peaks but instead two rutile peaks (200) and (400) at 39.18° and 84.26°, respectively.

The best anatase-TiO_2(001)-(4×1) film on $LaAlO_3$(001) substrate with flat surface and well defined interface between film and substrate was obtained for sample temperature T = 680°C, oxygen pressure $p_{O2} = 5.0\times10^{-4}$ mbar, laser energy 44 mJ, laser pulse frequency 5 Hz, and sample target distance 47 mm (Fig. 2 – Fig. 5, Table 1- sample g). Figure 2(a) shows a RHEED pattern of the anatase-TiO_2(001)-(4×1) surface taken along [100] azimuthal direction. The streakiness of the pattern suggests that the film surface is now well ordered and flat. Aside from the primary 1× RHEED diffraction pattern, weak 4× diffraction features consisting of three additional streaks within each 1× structure were also visible, suggesting that a 4× reconstruction occurred along [010] direction during the growth. The additional 1/4-order peaks in Fig. 2(c) are symmetrically positioned, showing equal distances between each other and the fundamentals. Further, LEED was used to examine the anatase-TiO_2(001)-(4×1), Fig. 2(b). A two domain structure, concerning of (1×4) and (4×1) of TiO_2 is clearly evident. The profile in Fig. 2(d) represents the intensity of spots along (-1 1) – (1 1) direction

with clearly visible maxima corresponding to (1×4) and (4×1) reconstruction. Similar TiO_2 reconstruction was observed on $SrTiO_3$ substrate [28, 33]. The XRD 2θ-θ scan in Figure 3(a) shows well defined sharp anatase (00*l*) peaks, indicating that a pure anatase film is formed, and that the film is preferentially aligned. The full width at half maximum (FWHM) of the (004) anatase peak rocking curve, Fig. 3(b), is 0.34° while that of anatase film fabricated on $SrTiO_3$(001) substrates is larger than 0.6° [34]. Thus the effect of lattice mismatch is clearly reflected in the crystal quality. The difference between growth conditions for the sample in Fig. 1(b) and the best grown sample in Fig. 3(b) from rocking curve experiment has shown that in case of sample "Fig. 1(b)" FWHM = 0.57° and for sample "Fig. 3(b)" 0.34° as was reported above. Those differences could suggest that the anatase film in Fig. 1(b) has some kind of microstrine. Only a near perfect crystal structure would produce very sharp peaks observed when the crystal is perfectly tilted. In addition, a decrease of the period of oscillation in the fringes diffraction intensity correlated with the film thickness increase was observed. The measured surface roughness from AFM image, Figure 4(a), was found to be 0.43 nm. Hence, the TiO_2 film seems to uniformly cover the substrate.

The room temperature STM image of the anatase-TiO_2(001)-(4×1) surface, Figure 4(b), shows a 2D surface with a stepped structure. Only two preferred step directions in the crystographically equivalent (100) and (010) directions were observed. The height of these steps on the TiO_2(001)-(4×1) surface was measured by STM in Figure 4(c) to be 0.5 nm and 0.25 nm, respectively. These values correspond to two and one atomic-layer height steps and are in agreement with our STEM results in Fig. 5(a)-(b) [35]. Analysis of the frequent existence of steps with a single atomic-layer height suggests that the anatase-TiO_2(001) surface exhibits two different surface truncations. It is expected, that these two truncations should have different surface structures as was observed for TiO_2 on $SrTiO_3$(001) [25, 33, 36].

The quality of these data described above indicated that the TiO_2 thin film is a high-quality single crystal with an anatase structure. However, detailed STEM analysis revealed the presence of numerous domains in the thin film, indicating the existence of domain boundaries not only from the epitaxial growth either side of terrace steps but also within an individual terrace. Figures 5(a) and 5(c) corresponds to Annular Dark Field (ADF) STEM images of the anatase-TiO_2(001)-(4×1) onto $LaAlO_3$(001) substrate.

The interface is determined based on the arrangement of atomic columns in bulk $LaAlO_3$ and TiO_2, confirms the formation of a clean and atomically abrupt interface between the two oxides, which means that the crystalline and epitaxial anatase TiO_2 phase on $LaAlO_3$ substrate was successfully produced. ADF images exposes the chemical composition in the heteroepitaxy since the intensity of the atomic columns scales as approximately $Z^{1.7}$, where Z is the average atomic number. Therefore the contrast is dominated by the cations with higher atomic number, and the oxygen atoms are not visible. The interface in the system strongly indicates an LaO-terminated layer [37], where the layer of LaO makes direct contact to a TiO_2 layer with the interfacial Ti sitting above hollow sites of the surface unit of LaO for domain II correspond to (001)[010]TiO_2//(001)[001] $LaAlO_3$ and above on top sites for domain I correspond to (001)[001]TiO_2//(001)[001] $LaAlO_3$. Those domains are related by a 90° rotation of the anatase and/or n/4 a[001] (=[010]) translation. In Figure 5(c) three types of domain boundaries that could be distinguished within the TiO_2 thin film based on the epitaxial growth relationship mentioned above are shown. Figure 5(b) represents a structural model of the first type of domain, with the same orientation on the atomically flat LaO-terminated substrate surface with the substrate terraces observed in Figure 5(a) [20]. No any changes in the first domain in the relationship to two different atomic steps were observed. From the STEM experiment, one atomic layer of TiO_2 along the c-axis corresponds to 1/4 of the unit cell, Fig. 5(b) [38, 36]. This result is in good agreement with our STM studies, shown

in Figures 4(b) and (c). The second domain can be described as 90° rotation plus a relative shift of a [001] $LaAlO_3$ (the terrace height), which is approximately equal to c3/8 [001] of TiO_2. An example is seen in the ADF-STEM image in Figure 5(c), with its structural model in Figure 5(d). The third additional observed domain boundary type in Figure 5(c) is not connected with the layer step from substrate but is the superposition of rotation and tilt of anatase phases. Those domains can also be preferential sites for the segregation of dopants, which can be similar to the role of grain boundaries in nano-crystalline anatase [39]. These domains appear to be common to all single-crystal anatase TiO_2 thin films grown on $LaAlO_3$, since all substrate have terraces and even without the presence of terrace steps, rotation domains are able to form inside the bulk crystal.

The growth parameters including: the KrF pulsed laser frequency; laser energy density; and oxygen pressure during deposition, all play a crucial role in the formation of proper epitaxial TiO_2 phase. The geometry of the ultra-high vacuum pulsed deposition system (including the sample holder to target distance), Fig. 6, affects the material transport between the target and the substrate. The substrate temperature influences the thermodynamic equilibrium for the well-defined epitaxial growth of atomically flat surfaces. Furthermore, the correct stoichiometry of the substrate surface (in this case $LaAlO_3$) during heating, deposition and cooling to the room temperature after deposition, ensures the use of the proper oxygen pressure. Further, the proper shape of the laser ablation plume corresponds to well-chosen laser energies and the oxygen pressures. By contrast, the improper selection of the above mentioned parameters leads to disordered epitaxial growth of TiO_2 phase with poor quality of surface layer, e.g. Fig.1(c). It should be pointed out, that growth characterisation with the use an ideally selected set of experimental methods (e.g. RHEED, LEED, XRD, AFM, STM, and STEM) play a key role in finding the most appropriate growth conditions.

4. CONCLUSIONS

In summary, it has been shown that the degree of order of epitaxial anatase-TiO_2 thin films can be manipulated by varying growth parameters such as the sample temperature, sample to target distance, oxygen pressure, laser energy, and laser pulse frequency. Optimisation of the epitaxial growth of TiO_2 thin films on $LaAlO_3$(001) substrates was performed with the use of ultra-high vacuum PLD, and investigated by RHEED, LEED, XRD, AFM, STM, and STEM. The results obtained clearly demonstrate that the TiO_2 thin film, which covers the entire substrate, has a distinctly anatase phase, and can be atomically aligned and bonded to $LaAlO_3$(001) substrate. Anatase-TiO_2 thin films showed high crystalline quality, evidenced by RHEED, XRD, LEED, and atomic resolution STEM. Two, very well ordered domains (1×4) and (4×1) surface reconstruction of anatase were observed by RHEED and LEED. An analysis of the STM measurements indicates the coexistence of atomic steps of both 2.5 Å and 5 Å, confirming the existence of two TiO_2 domains. The STEM images also reveal that the interface is most likely terminated with a LaO layer.

ACKNOWLEDGMENTS

K. Krupski acknowledges the support of the Engineering and Physical Sciences Research Council (EPSRC) for the award of a DTA studentship. A. Krupski was partially supported by the University of Portsmouth under Start Up Fund 44327/2015.

References

[1] R. Asahi, T. Morikawa, T. Ohwaki, K. Aoki, and Y. Taga, Science, **293** (2001) 269.

[2] O. Carp, C.L. Huisman, and A. Reller, Prog. Solid State Chem. **32** (2004) 33.

[3] C. J. Barbe, F. Arendse, P. Comte, M. Jirousek, F. Lenzmann, V. Shklover, and M. Gratzel, J. Am. Ceram. Soc. **80** (1997) 3157.

[4] W. Zhou, F. F. Sun, K. Pan, G. H. Tian, B. J. Jiang, Z. Y. Ren, C. G. Tian, and H. G. Fu, Adv. Functional Mater. **21** (2011) 1922.

[5] T.B. Song, Q. Chen, H. Zhou, C. Jiang, H.H. Wang, Y. Yang, Y. Liu, J. You, and Y. Yang, J. Mater. Chem. A **3** (2015) 9032.

[6] D.P. Woodruff (ed.) *The Chemical Physics of Solid Surface, Vol. 9 Oxide Surfaces* (Elsevier, Amsterdam, 2001).

[7] U. Diebold, Surf. Sci. Rep. **48** (2003) 53.

[8] M.A. Henderson, Surf. Sci. Rep. **46** (2002) 5.

[9] C.L. Pang, R. Lindsay, and G. Thornton, Chem. Soc. Rev. **37** (2008) 2328.

[10] G.S. Herman, M.R. Sievers, and Y. Gao, Phys. Rev. Lett. **84** (2000) 3354.

[11] V. F. Silva, V. Bouquet, S. Deputier, S. Boursicot, S. Ollivier, I. T. Weber, V. L. Silva, I. M. G. Santos, M. Guilloux-Viry, and A. Perrin, J. Appl. Crystallogr. **43** (2010) 1502.

[12] A. Lotnyk, S. Senz, and D. Hesse, Thin Solid Films, **515** (2007) 3439.

[13] B.H. Park, J.Y. Huang, L.S. Li, and Q.X. Jia, Appl. Phys. Lett. **80** (2002) 1174.

[14] B.S. Jeong, J.D. Budai, and D.P. Norton, Thin Solid Films, **422** (2002) 166.

[15] X. Weng, P. Fisher, M. Skorwronski, P.A. Salvador, and O. Maksimov, J. Cryst. Growth, **310** (2008) 545.

[16] J.Y. Huang, B.H. Park, D. Jan, X.Q. Pan, Y.T. Zhu, and Q.X. Jia, Phil. Mag. A, **82** (2002) 735.

[17] M. Murakami, Y. Matsumoto, K. Nakajima, T. Makino, Y. Segawa, T. Chikyow, P. Ahmet, M. Kawasaki, and H. Koinuma, Appl. Phys. Lett. **78** (2001) 2664.

[18] M. Zhu, T. Chikyow, P. Ahmet, T. Naruke, M. Murakami, Y. Matsumoto, and H. Koinuma, Thin Solid Films, **441** (2003) 140.

[19] H. Sakama, G. Osada, M. Tsukamoto, A. Tanokura, and N. Ichikawa, Thin Solid Films, **515** (2006) 535.

[20] S. Zheng, C.A.J. Fisher, T. kato, Y. Nagao, H. Ohta, and Y. Ikuhara, Appl. Phys. Lett. **101** (2012) 191602.

[21] R. Ciancio, A. Vittadini, A. Selloni, R. Arpaia, C. Aruta, F.M. Granozio, U.S. di Uccio, G. Rossi, and E. Carlino, J. Nanopart. Res. **15** (2013) 1735.

[22] S. Yamamoto, T. Sumita, T. Yamaki, A. Miyashita, and H. Naramoto, J. Cryst. Growth, **237** (2002) 569.

[23] S. Kitazawa, Y. Choi, S. Yamamoto, and T. Yamaki, Thin Solid Films, **515** (2006) 1901.

[24] S.A. Chambers, C.M. Wang, S. Thevuthasan, T. Droubay, D.E. McCready, A.S. Lea, V. Shutthanandan, and C.F. Windisch Jr., Thin Solid Films, **418** (2002) 197.

[25] Y. Liang, S.P. Gan, S.A. Chambers, and E.I. Altman, Phys. Rev. B, **63** (2001) 235402.

[26] M. Lazzeri, and A. Selloni, Phys. Rev. Lett. **87** (2001) 266105.

[27] Y. Wang, H.J. Sun, S.J. Tan, H. Feng, Z.W. Cheng, J. Zhao, A.D. Zhao, B. Wang, Y. Luo, J.L. Yang, and J.G. Hou, Nature Comm. **4** (2013) 2214.

[28] G.S. Herman, M.R. Sievers, and Y. Gao, Phys. Rev. Lett. **84** (2000) 3354.

[29] R. Hengerer, B. Bolliger, M. Erbudak, and M. Gratzel, Surf. Sci. **460** (2000) 162.

[30] M. Lazzeri, A. Vittadini, and A. Selloni, Phys. Rev. B **63** (2001) 155409.

[31] K.J. Krupski, M. Moors, P. Jóźwik, T. Kobiela, and A.R. Krupski, Materials **8** (2015) 2935.

[32] I. Horcas, R. Fernández, J.M. Gómez-Rodríguez, J. Colchero, G. Herrero, and A.M. Baro, Rev. Sci. Instrum. **78** (2007) 013705.

[33] M. Radovic, M. Salluzzo, Z. Ristic, R. Di Capua, N. Lampis, R. Vagilo, and F. Mietto Granozio, J. Chem. Phys. **135** (2011) 034705.

[34] A. Lotnyk , S. Senz, and D. Hesse, Thin Solid Films, **515** (2007) 3439.

[35] T. Luttrell, S. Halpegamage, E. Sutter, and M. Batzill, Thin Solid Films **564** (2014) 146.

[36] Y. Du, D.J. Kim, T.C. Kaspar, S.E. Chamberlin, I. Lyubinetsky, and S.A. Chambers, Surf. Sci. **606** (2012) 1443.

[37] Z. Wang, W. Zeng, L. Gu, M. Satio, S. Tsukimoto, and Y. Ikuhara, J. Appl. Phys. **108** (2010) 113701.

[38] M. Murakami, Y. Matsumoto, and K. Nakajima, Appl. Phys. Lett. **78** (2001) 2664.

[39] B.P. Uberuaga, and X.M. Bai, J. Phys: Condens. Matter, **23** (2011) 435004.

FIGURE CAPTIONS:

Fig.1. RHEED, AFM, XRD and HRXRD results of TiO_2 on $LaAlO_3$(001) - Samples A-F (described in Table 1). The quality of the TiO_2 thin films depends strongly on the growth conditions. (a) sample A – different laser energy; (b) sample B – different sample-target distance; (c) sample C – oxygen pressure changed during sample annealing; (d) sample D – sample temperature during growth T = 670 °C; (e) sample E – sample temperature during growth T = 690 °C; (f) sample F – different laser pulse frequency.

Fig. 2. Anatase TiO_2 on $LaAlO_3$(001) - Sample G. (a) The RHEED pattern along [100] direction. In addition to the 1× diffraction features, a weak 4× diffraction pattern consisting of three additional lines within the 1× pattern are visible; (b) LEED patterns of a two-domain (4×1) reconstructed surface recorded at normal electron incidence for E = 90 eV, and T = 300 K; (c) profile along the line A in the RHEED (a) showing equally spaced 1/4-order peaks between the fundamental peaks; (d) line profile from LEED pattern along (-1 1) – (1 1) direction with maxima from the (1×4) and (4×1) reconstructions.

Fig. 3. XRD scans from anatase TiO_2 on $LaAlO_3$(001) - Sample G. (a) the 2θ-θ scan and (b) rocking curve.

Fig. 4. Anatase TiO_2 on $LaAlO_3$(001) - Sample G. (a) nc-AFM (10 000 Å × 10 000 Å); (b) STM image (2 500 Å × 2 500 Å, I_T = 0.5 nA, U_{bias} = 1.0 V) showing a continuous anatase film formed by the coalescence islands; (c) line scan along the line B from the image in (b) demonstrating that the height of the TiO_2(001) layers corresponds to the height of 0.25 and 0.5 nm, respectively.

Fig. 5. Anatase TiO_2 on $LaAlO_3$(001) - Sample G. (a) STEM image and (b) corresponding schematic of [010] boundary formed on step terrace with highest equal to 1/4c = 2.5 Å; (c) STEM image with three different domains and (d) corresponding schematic of mixed type of domain I and II boundaries formed by 90° rotation plus a relative shift of α [001] $LaAlO_3$ due the substrate terrace and domain III which is not connected with the substrate.

Fig. 6. Geometry of the ultra-high vacuum pulsed laser deposition system: (1) KrF pulsed laser beam, (2) sample holder, (3) stainless steel sample plate, (4) $LaAlO_3$(001) sample, (5) TiO_2 target, (6) laser ablation plume, (7) RHEED screen.

Table 1.
Growth parameters of TiO_2 thin films on $LaAlO_3$(001) surface.

FIGURES

Fig. 1.

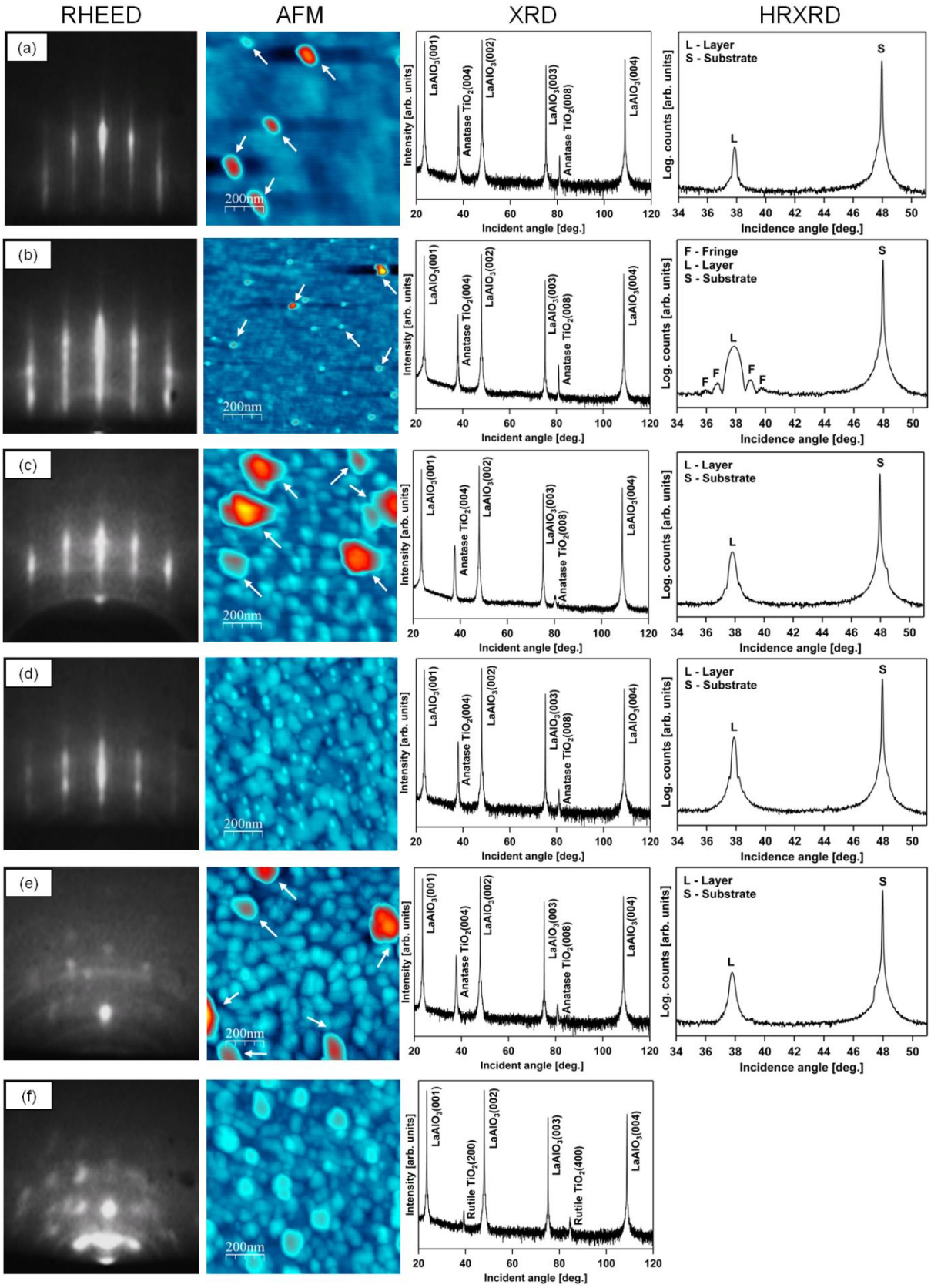

Fig. 2.

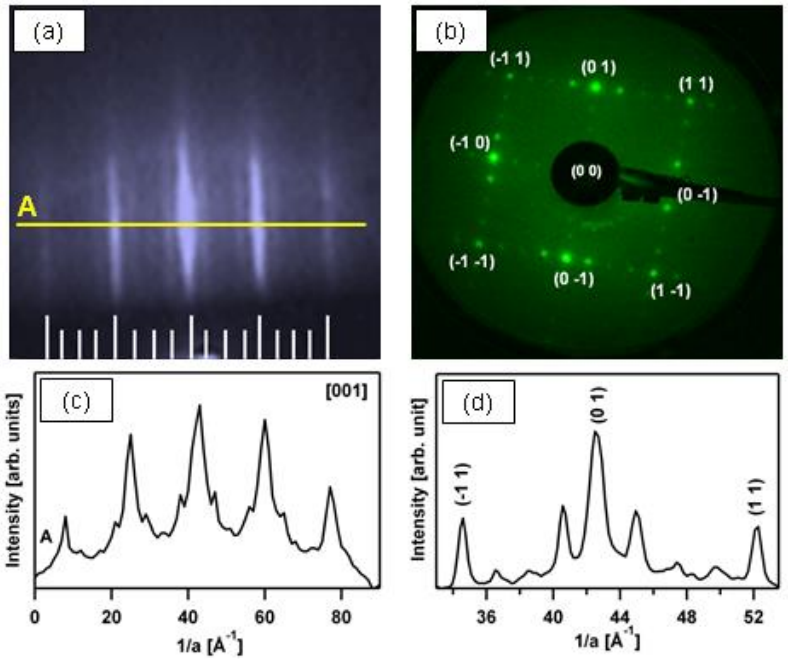

Fig. 3.

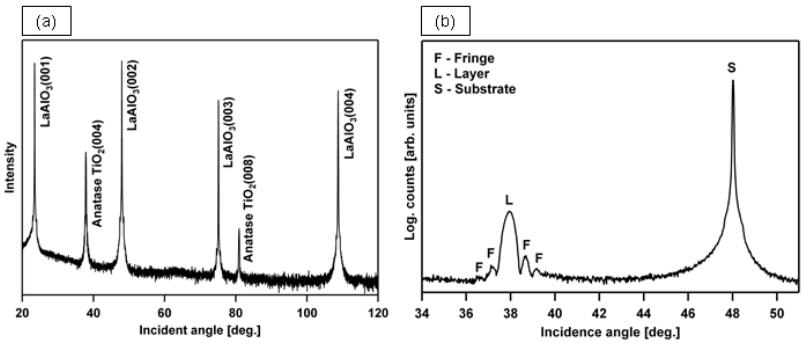

Fig. 4.

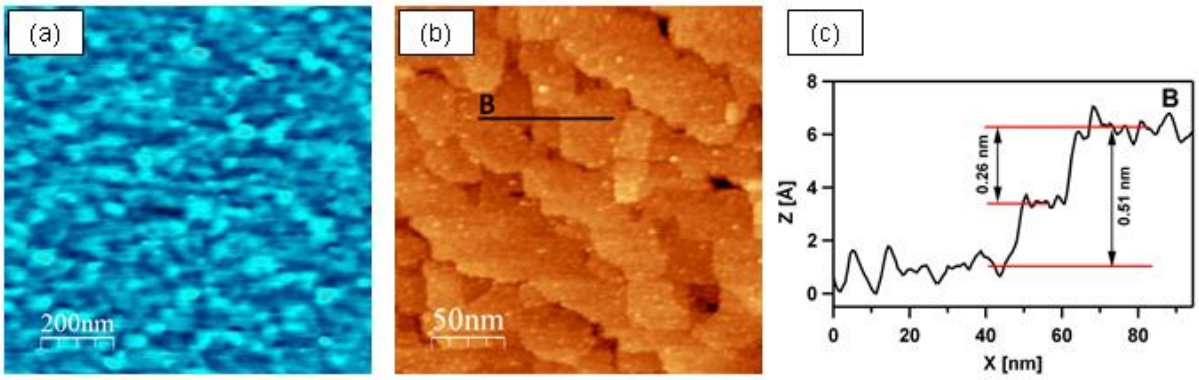

Fig. 5.

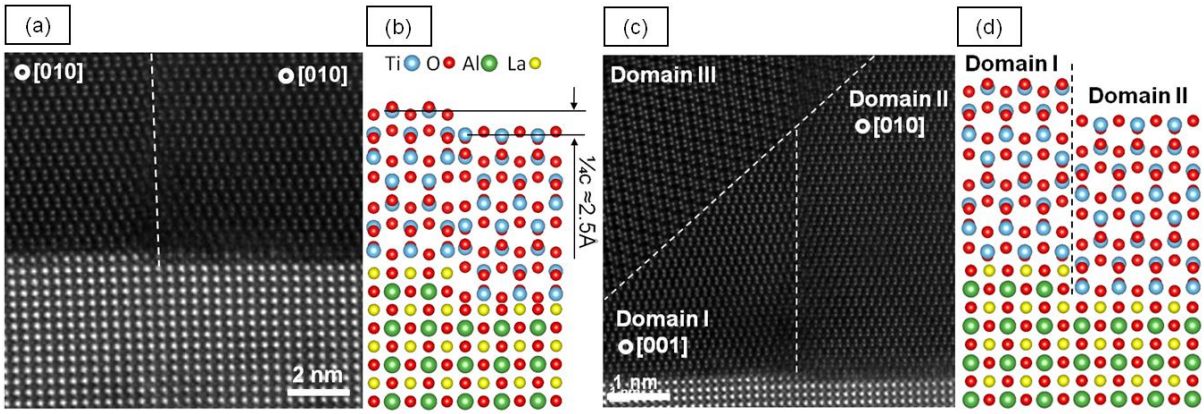

Fig. 6.

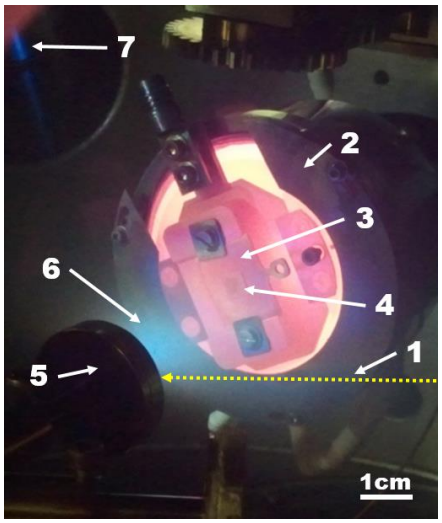

Table 1

Sample	*Sample Temperature [°C]*	*Oxygen Pressure during annealing [mbar]*	*Laser Energy [mJ]*	*Laser Pulse Frequency [Hz]*	*Sample – Target Distance [mm]*	*TiO_2 Layer Thickness [nm]*			*TiO_2 Layer Roughness from AFM [nm]*
						HRXRD	*XRR*	*TEM*	
A	680	5×10^{-4}	43	5	47	-	66.90	60.50	1.65
B	680	5×10^{-4}	44	5	57	9.00 ±0.70	8.80	10.70	0.72
C	680	1×10^{-1}	44	5	47	-	31.43	-	9.00
D	670	5×10^{-4}	44	5	47	-	46.92	47.60	3.40
E	690	5×10^{-4}	44	5	47	-	100.26	-	9.30
F	680	5×10^{-4}	44	8	47	-	7.64	-	7.20
G	680	5×10^{-4}	44	5	47	19.60 ±0.20	19.39	20.5	0.43